CHAPTER 4

Synthesis and Photocatalytic application of magnetically recyclable starch functionalized Fe_3O_4/Cu_2O nanostructures

4.1 Introduction

The improper disposal of industrial wastes has led to the contamination of limited sources of drinking water. A significant portion of residues from chemical industries contain phenol-based compounds and organic dyes that are exceedingly stable under natural conditions [Fortuny *et al.* (1999), Christoskova *et al.* (2001), Robinson *et al.* (2001), Zhang *et al.* (2009)]. One of these, p-nitrophenol (PNP), is a prominent, highly durable, carcinogenic toxic organic waste [Dohnal *et al.* (1995), Environmental Protection Agency (2000)]. Photo-Fenton reactions on wide bandgap photocatalysts like TiO_2, ZnO, WO_3, and ZnS have been used for the degradation of PNP. Photo-excitation of these semiconductors requires UV light, which is only a minor component of the solar spectrum [Shaoqing *et al.* (2010), Khatamian *et al.* (2012), Zarei *et al.* (2020), Torres-Martínez *et al.* (2001)]. Only a few publications in literature have investigated visible light photocatalysts for the photo-Fenton degradation of PNP [Guo *et al.* (2013), Yoon *et al.* (2017), Zeng *et al.* (2017), Pal *et al.* (2020)].

Since the recovery of nanocatalysts at the industrial scale is a costly affair; therefore, their recyclability is crucial. An economical way of tackling this problem is to use superparamagnetic photocatalysts [Lv *et al.* (2016), Shao *et al.* (2019)]. The application of an external magnetic field can easily separate the photocatalyst particulates from the solution phase. Re-dispersal of the photocatalyst can be achieved just by removing the magnetic field. Given the advantages, the present research attempts to develop a superparamagnetic visible light photocatalyst for PNP degradation.

A visible light photocatalyst that demonstrates effective charge separation and easy recyclability should be a nanocomposite made of magnetic and non-magnetic semiconducting components. Both parts must have bandgaps suitable for harnessing visible light energy properly. Moreover, the valence band (VB) and conduction band (CB)

positions of the non-magnetic component should be staggered relative to the magnetic semiconductor part to enable proper charge separation.

The spinel structured magnetite (Fe_3O_4), a well-known Fenton catalyst [Rusevova *et al.* (2012), Hou *et al.* (2014)], could be the magnetic component in such a nanocomposite. Bulk magnetite has a very small bandgap (~0.1 eV). The bandgap of this n-type semiconductor increases substantially (1.8-2.2 eV) when the size decreases to nano-range due to the quantum size effect [Xu *et al.* (2000), Smith *et al.* (2010)]. Magnetite also exhibits superparamagnetic behavior in the appropriate nano-size range. Natural magnetite has been used to catalyze the Fenton degradation of PNP. However, the rate of such degradation is relatively slow [Hongping *et al.* (2015)]. There are some reports on the photo-Fenton degradation of PNP by nanocomposites obtained by combining the magnetite part with wide bandgap semiconductors like TiO_2, ZnO, etc. [Hou *et al.* (2016), Qin *et al.* (2017)]. But these are activated only by UV light.

Cuprous oxide (Cu_2O), a p-type semiconductor with a visible range bandgap in the 2-2.5 eV range, is an economical option for the non-semiconducting part of the desired nanocomposite. Its VB and CB positions are staggered relative to nano-Fe_3O_4. Nanoparticles of Cu_2O have been utilized as visible light photocatalysts for the degradation of organic pollutants but generally get deactivated due to photo corrosion [Huang *et al.* (2009)]. Charge separation by combining Cu_2O with another component can solve this problem. Thus, many researchers have successfully used nanoparticles of Cu_2O decorated with noble metal (e.g., Au, Ag, Cu, and Pt) nanostructures to degrade organic dyes [Yang *et al.* (2014), Ai *et al.* (2009), Lu *et al.* (2016), Gong *et al.* (2018)]. Heterojunction photocatalysts formed by joining Cu_2O with other semiconductors like

TiO_2, ZnO, CuO, and MoS_2 have also been used to degrade organic dyes [Kaviyarasan *et al.* (2019), Wu *et al.* (2017), Jiang *et al.* (2017), Li *et al.* (2020)].

There is little research on the fabrication of magnetically reusable visible light photocatalysts for the degradation of toxic organic pollutants like PNP. Magnetic recyclability can make such photocatalysts viable for industrial use. Therefore, the present research investigates starch functionalized Fe_3O_4/Cu_2O (CF) nanocomposite for the photo-Fenton degradation of PNP and methyl orange (MO) under visible light irradiation. The stabilization of magnetite by soluble starch (*s*-Fe_3O_4) facilitates the preparation of nanoparticles in the 10- 20 nm range and also improves their dispersibility in the aqueous medium considerably [Singh *et al.* (2015)]. Organic modifiers like starch affect the morphology and size of the Fe_3O_4 nanoparticles, thereby their optical bandgap value [Radoń *et al.* (2017)]. The joining of p-type Cu_2O with n-type magnetite results in a p-n junction that improves the charge separation and, hence, photocatalytic activity towards photo-Fenton degradation of PNP and MO.

4.2 Experimental

4.2.1 Preparation of starch functionalized magnetite nanoparticles (SMNPs)

As discussed in section 3.2.1.

4.2.2 Synthesis of SMNPs/ Cu_2O (CF) nanocomposites

60 mg of SMNPs nanoparticles were re-dispersed in 60 mL of distilled water. An aqueous suspension of re-dispersed SMNPs and 25 mL of 0.01 M $Cu(NO_3)_2.3H_2O$ (Merck) was prepared and allowed to stand at 60 ^{0}C for 24 hours to achieve adsorption equilibrium. After the adsorption step, an appropriate amount of 0.5M glucose (Merck) solution was added to the suspension. The resultant suspension was then added in a drop-wise manner to 50 mL of 1 M NaOH with constant heating at 80 ^{0}C and stirring. The

prepared nanocomposite (CF) precipitate was magnetically separated and washed several times with distilled water until the washings turned neutral, and then dried (at 40^oC) in a hot air oven.

4.2.3 Photocatalytic degradation of PNP over CF nanocomposites

For photocatalytic degradation investigations on CF, 50 µL catalyst (from 1mg in 1mL distilled water) suspension was mixed with 2mL of PNP (0.2mL of 176µM diluted with 2 mL distilled water) solution at pH 3. The PNP solution's pH was maintained by adding required volumes of 0.1M HCl or 0.1 M NaOH solutions. The suspension was then kept for adsorption (for 60 minutes) until equilibrium. Then, 50µL of 2 M H_2O_2 (Merck) solution was added to this suspension. The reaction was conducted both in the dark and under visible light from the cool white LED (0.1470 watts/cm^2) to compare the Fenton and photo-Fenton activities of CF catalysts.

4.2.4 Photocatalytic degradation of methyl orange over CF nanocomposites

For catalytic degradation of MO over CF, 100 µL of the dispersed catalyst (1mg in 1mL distilled water) was added into 2mL of the 140µM solution of MO at pH 3. This suspension was then kept for adsorption (for 60 minutes) until equilibrium was achieved. Next, 10µL of 2 M H_2O_2 solution was added to the reaction mixture. The rest of the procedure was the same as that in the previous sub-section.

4.2.5 Analysis

The X-ray diffraction patterns of the samples were recorded on the Rigaku Miniflex 600 instrument. The CF samples' TEM imaging was carried out with FEI Technai-20 G2, operating at a voltage of 200 kV. The solid-state UV-visible measurement was performed on the Shimadzu Pharmaspec UV-1700 model, working in the 200−800 nm spectral range.

X-ray photoelectron spectroscopy (XPS) was carried out on a Thermo Fisher Scientific K-alpha instrument. The pass energy for the survey scan detector was 1 eV, while it was 0.10 eV for high-resolution spectra recordings. All spectra were referenced to adventitious carbon signal at 284.8 eV and fitted using GL (30) line shape for all peaks with Casa XPS software from Casa Software Ltd. CH instrument model CHI-7044 was used for the electrochemical analysis. SMNPs and CF's magnetization curves were measured using the Magnetic Property Measurement System (MPMS3)-SQUID VSM. UV-visible absorption spectra measurements, during the catalytic experiment, were done on Agilent Cary 60 spectrophotometer.

4.3 Results and discussion

4.3.1 Characterization

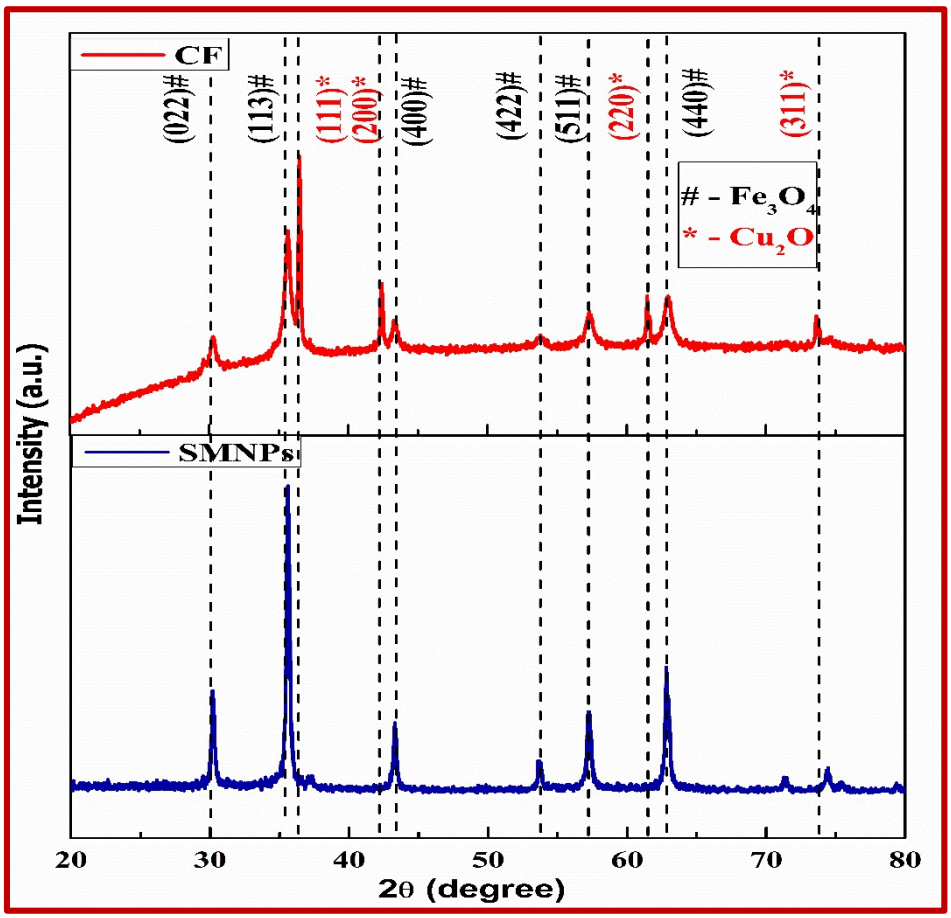

Figure 4.1 The X-ray powder diffraction pattern of SMNPs and CF powder samples.

Figure 4.1 compares the powder X-ray diffraction patterns of SMNPs and CF nanostructures. The XRD pattern of CF nanostructures exhibit peaks corresponding to both Fe_3O_4 (JCPDS89-2355) and the Cu_2O (JCPDS78-2076) phases, indicating composite formation. The XRD peaks at 36.4°, 42.3°, 61.4°, and 73.5° (2θ) correspond to the Cu_2O phase. The rest of the peaks in the figure match those of the magnetite phase.

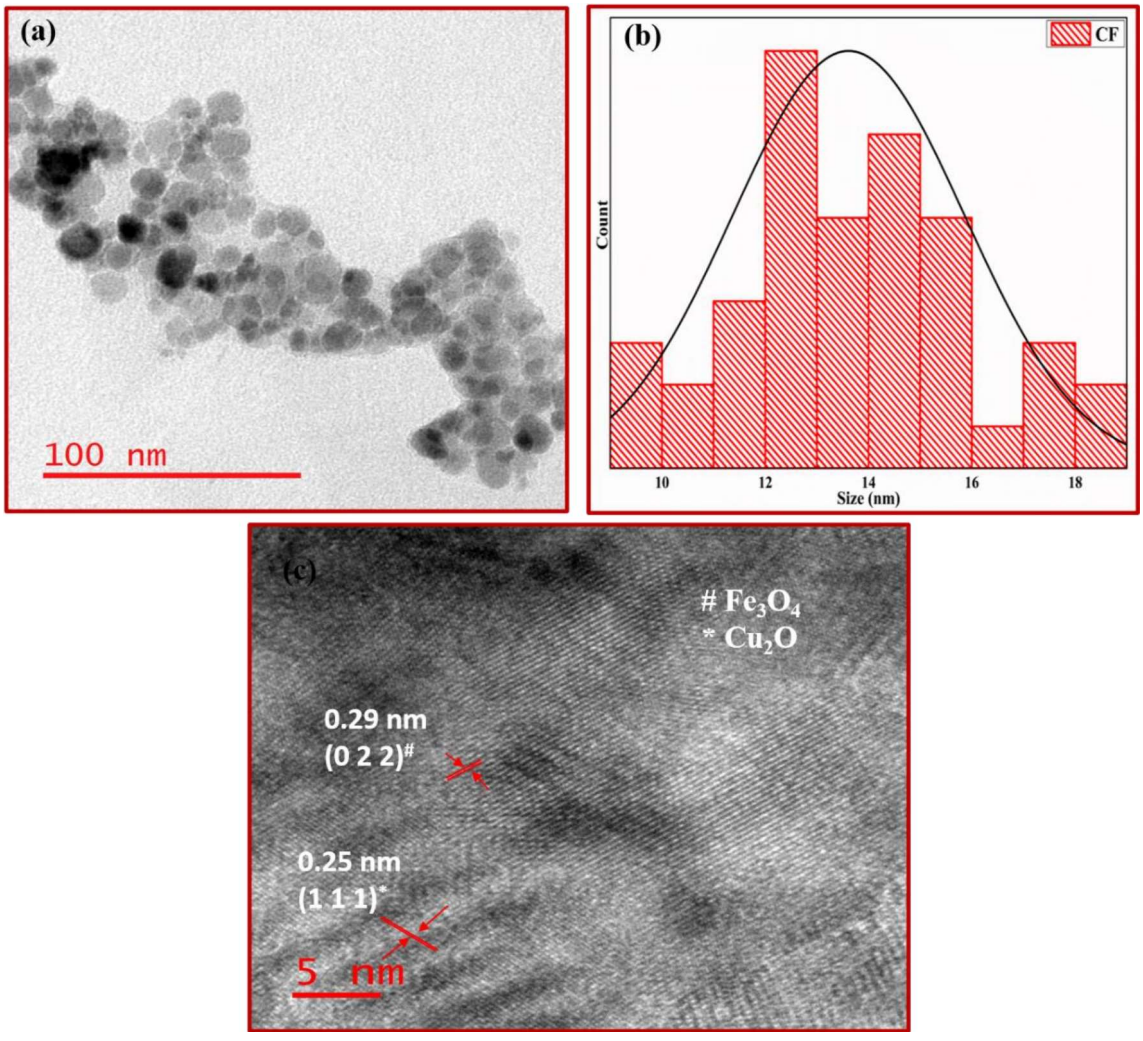

Figure 4.2 (a) Bright-field TEM image, **(b)** the size distribution plot, and **(c)** HR-TEM image of the CF nanostructure.

Figure 4.2(a) and 4.2(b) shows the bright-field TEM image of CF nanoparticles and their respective size distribution. The average size of the nanocomposite is ~13.5 nm.

Figure 4.2(c) displays a typical HR-TEM image of nanocomposite particles. The lattice spacings 0.29 nm and 0.25 nm correspond to the (022) plane of FCC Fe_3O_4 and (111) plane of cubic Cu_2O, respectively. Adjacently located FCC Fe_3O_4 and cubic Cu_2O phases confirmed the formation of the CF nanocomposites.

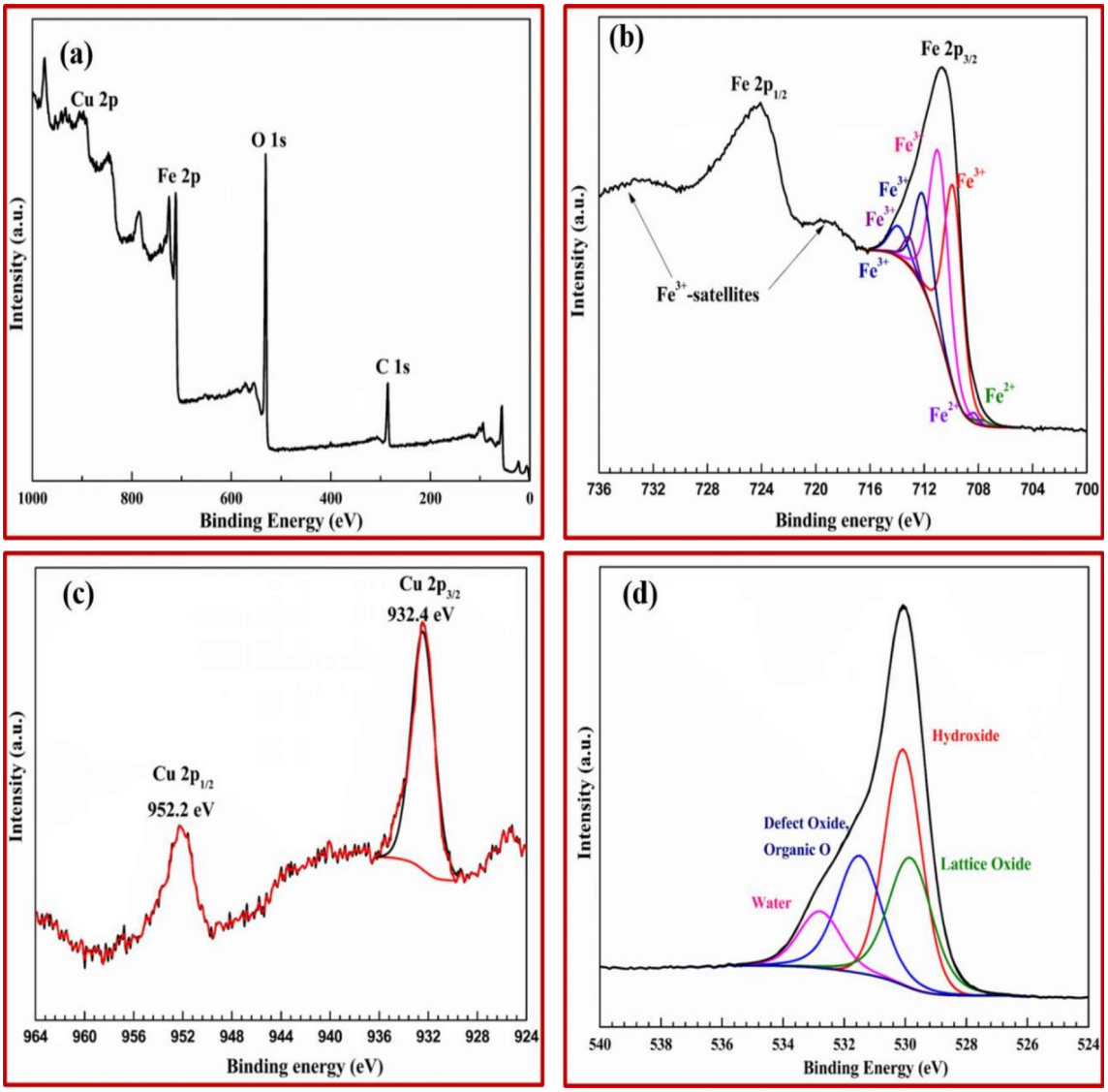

Figure 4.3 XPS analysis of CF **(a)** survey spectrum **(b)** Fe 2p, **(c)** Cu 3d, and **(d)** O 1s.

The presence of Cu_2O, along with Fe_3O_4 in CF, was also confirmed by its XPS spectrum (Figure 4.3). Analysis of the survey spectrum shows the presence of carbon (32.78 %), oxygen (50.46 %), copper (2.46 %), and iron (14.3 %) in CF. Signals of Fe indicate that Cu_2O nanostructures only partially covered the magnetite surface. The Fe 2p

peak showed the typical composition for magnetite nanoparticles, consisting of Fe^{2+} and Fe^{3+} species, following the fitting parameters for mixed species of Biesinger and co-workers [Biesinger *et al.* (2011)]. The high-resolution XPS spectrum of Cu 2p exhibits peaks at 932.4 eV and 952.2 eV corresponding to Cu 2p3/2 and 2p1/2, respectively, which confirms the presence of copper(I) oxide [Ghijsen *et al.* (1988)]. The high-resolution spectrum of the O 1s region showed lattice oxide signals at 529.83 eV.

Figure 4.4 compares the magnetization versus magnetic field (M-H loop) plots at room temperature for SMNPs and CF nanoparticles. Both nanostructures show typical superparamagnetic hysteresis characteristics. The magnetic moment for CF nanocomposite was slightly lesser than that of SMNPs due to the precipitation of Cu_2O nanostructures on the starch stabilized magnetite surface. Even then, the saturation magnetization values for CF was sufficiently high for the nanoparticles to exhibit easy magnetic recyclability.

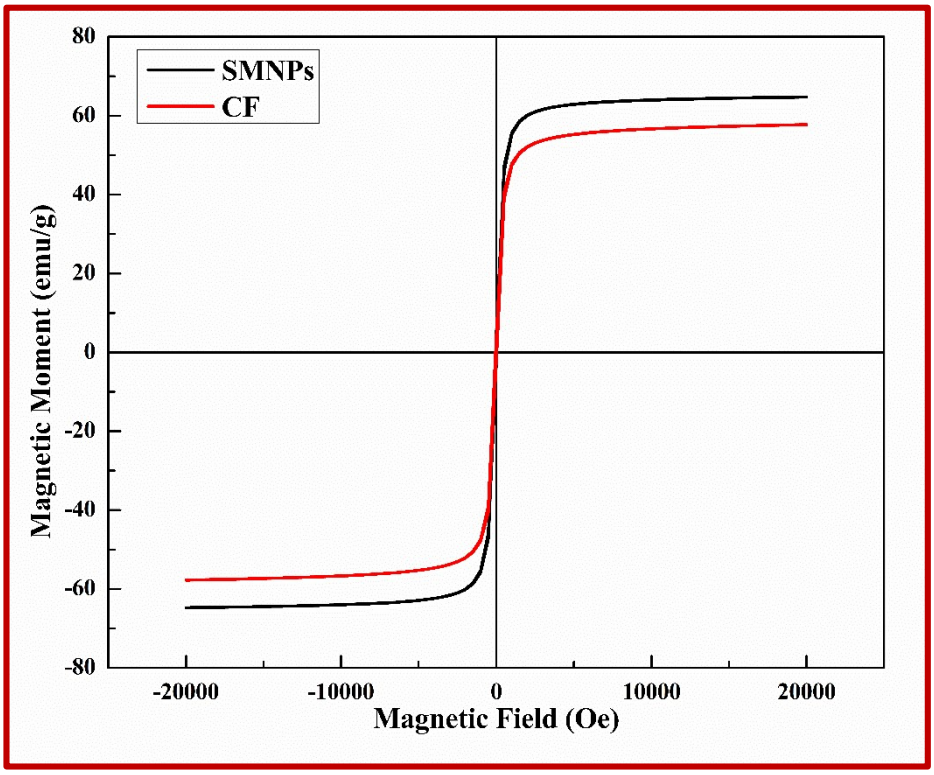

Figure 4.4 Magnetic moment versus magnetic field graph of SMNPs and CF.

4.3.2 Optical band determination

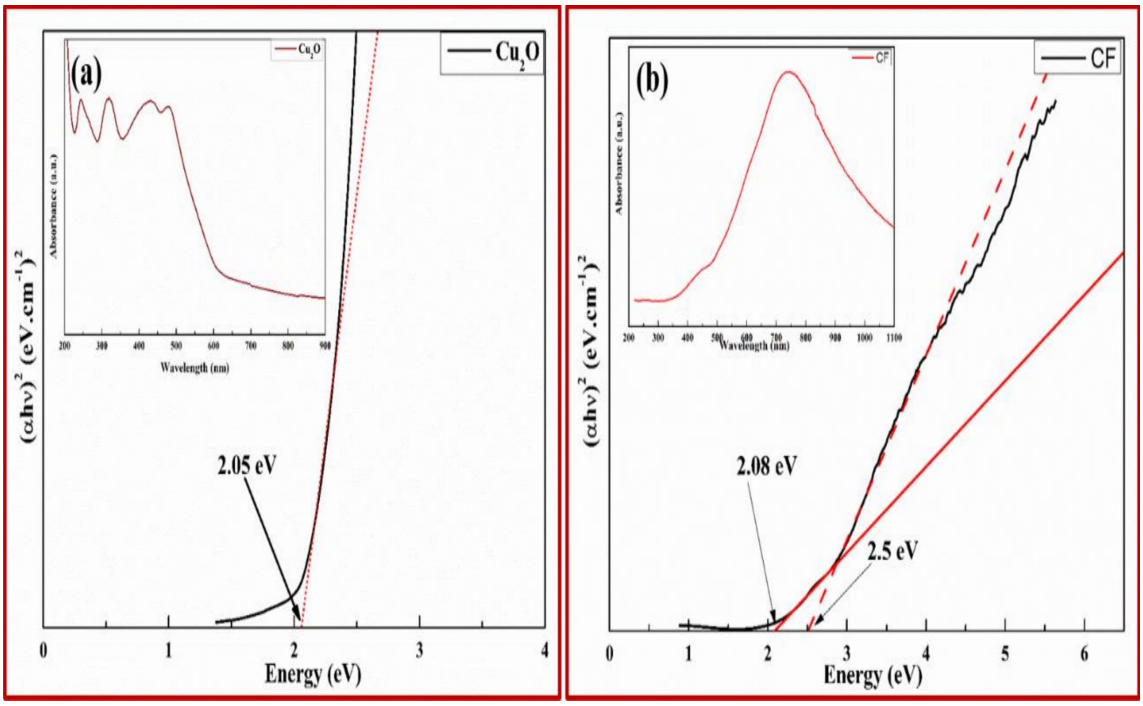

Figure 4.5 Tauc plot of pure **(a)** Cu_2O and **(b)** CF nanocomposite.

The determination of the possible photo-Fenton mechanism requires the knowledge of the optical bandgap of the nanomaterial. Tauc plots, drawn from the normalized solid UV-vis absorbance (Figure 4.5) data, were used to find the optical band gaps. The following equation gives the Tauc relation between the absorption coefficient alpha (α) and photonic energy (hυ) [Tumuluri *et al.* (2014)]

$$\alpha = \frac{1}{h\upsilon}(h\upsilon - E_g)^n \text{ or } (\alpha h\upsilon)^{1/n} = h\upsilon - E_g \qquad (2.2)$$

In the above equation, α is the molar absorption coefficient, n is the transition mode power factor, and E_g represents the semiconductor's bandgap energy. The exponent n is equal to 0.5 for allowed direct transition and 2 for the allowed indirect transition. The intercept of the linear fit to the plot on the x-axis gave the optical bandgap energy. There are two band gaps of 2.08 and 2.5 eV in the Tauc plot of sample CF. The bandgap at 2.08 eV is due to the magnetite portion. The bandgap at 2.5 eV is because of the Cu_2O component of the CF sample. A comparison with the pure Cu_2O shows a noticeable increase in the bandgap

of the Cu_2O part of the composite (Figure 4.5a). The quantum size effect due to the small size of Cu_2O nanostructures loaded on the SMNPs surface possibly causes the bandgap increase [Furukawa *et al.* (1988), Chen *et al.* (2018)].

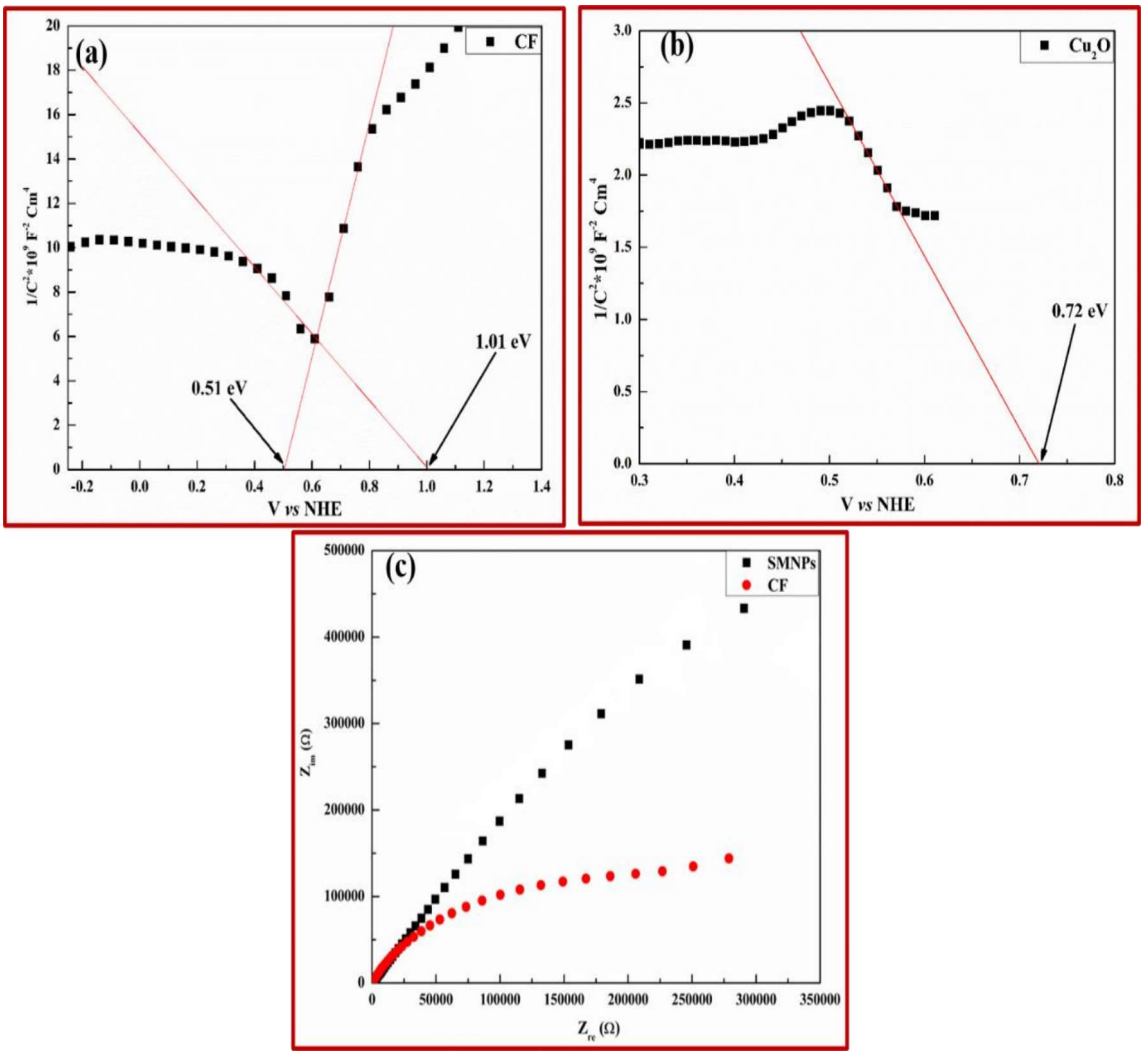

Figure 4.6 Mott Schottky plot of **(a)** CF and **(b)** Cu_2O measured under the dark condition in 0.5M Na_2SO_4 at 1 kHz and **(c)** the Nyquist plots of electrochemical impedance spectroscopy (EIS) for CF and SMNPs for the investigation of the electron transfer kinetics of the catalysts.

The Mott–Schottky (MS) plots of CF measured under dark condition (Figure 4.6a) gave the band edge positions of different parts of the composite. The MS plots of CF exhibited positive and negative slope parts, confirming a p-n heterojunction

formation. Flat band potential values obtained for CF were +0.50 eV vs. NHE and +1.01 eV vs. NHE. The potential vs. Ag/AgCl reference electrode was converted to the potential vs. NHE by the relation V(NHE) = V(Ag/AgCl) + 0.059 pH + 0.197 (here pH = 7). The schematic Figure 4.7a describes the relative band edge positions of pure starch functionalized magnetite component (SM) and Cu_2O materials. Part b of the same figure shows the positions of these band edges in the CF composite.

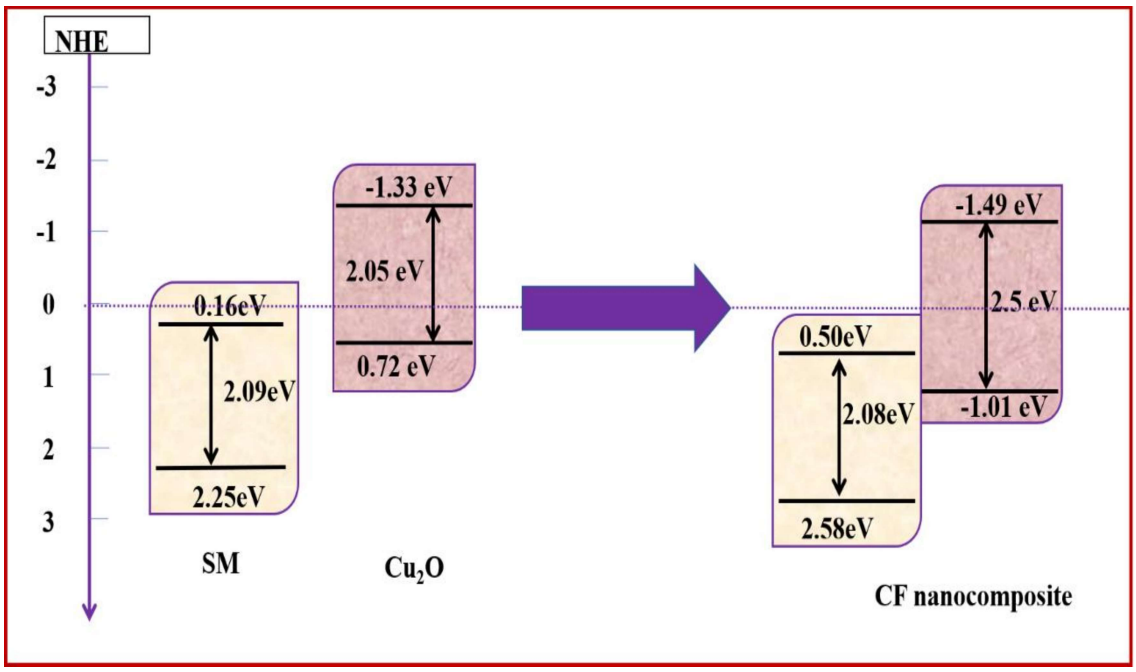

Figure 4.7 Bandgaps and band edge positions of **(a)** SM and Cu_2O pure materials **(b)** CF nanocomposite.

The formation of p-n junction shifts the positions of respective band edges. Figure 4.6c gives the Nyquist plots of electrochemical impedance spectroscopy (EIS) of SMNPs and CF. The smaller diameter of the semicircle in CF implies lower charge transfer resistance at the electrode/electrolyte surface [Wang *et al.* (2019), Liu *et al.* (2019)]. Therefore, the CF sample shows more efficient electron-hole separation than SMNPs.

4.3.3 Visible light photo-Fenton degradation of PNP and MO by CF nanocomposite

The photocatalysis experiments were performed at different pH to find out the optimum condition (figure 4.8). The degradation was faster in the acidic condition. Figure

4.9a shows the change in the UV-visible spectra of PNP, and Figure 4.10a displays the change in UV- visible spectra of MO in the presence of CF, H_2O_2, and visible light optimum pH 3. The UV-visible spectra of PNP and MO show a steady decrease in intensity with time. The disappearance of all peaks indicates PNP and MO's degradation to fragments that have no UV-visible signature.

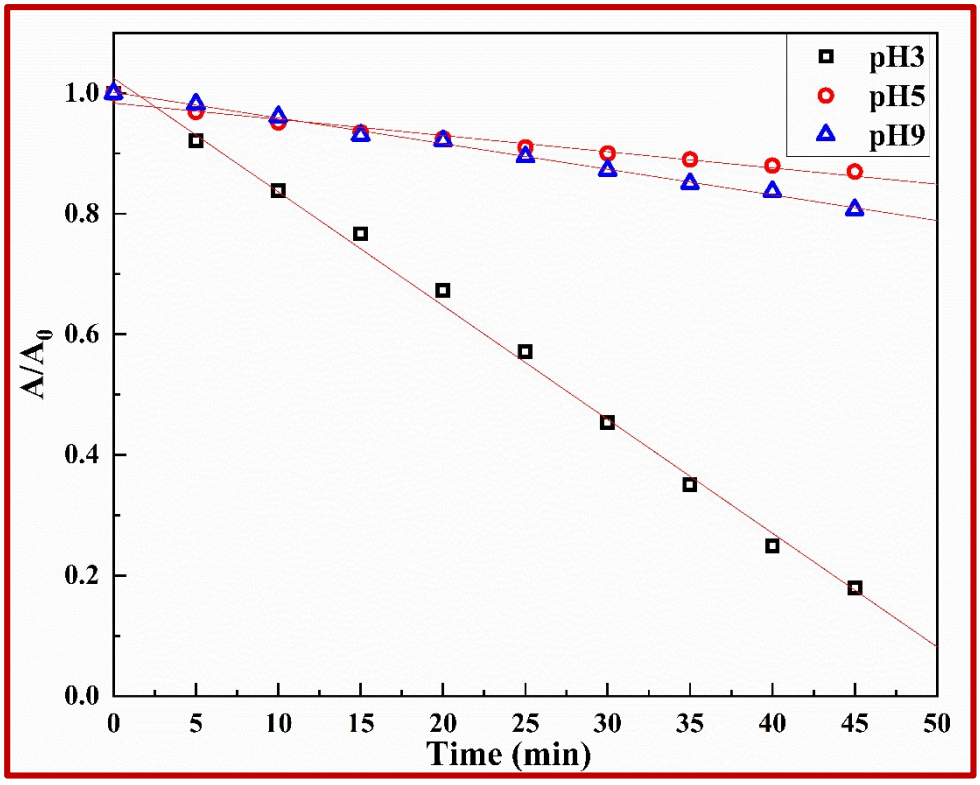

Figure 4.8 Kinetics of PNP degradation photocatalyzed by CF at different pH.

The differential rate law equation was used to investigate PNP and MO degradation kinetics by the photo-Fenton reaction [Alla *et al.* (2016)].

$$-\frac{\partial A_t}{\partial t} = k[H_2O_2]^m[A_t]^n \qquad (4.1)$$

The change in the concentration of H_2O_2 was negligible because of it being in excess. Making this approximation and substituting $k_{app} = k[H_2O_2]^n$ allows us to write equation 1 in the following manner.

$$-\frac{\partial A_t}{\partial t} = k_{app}[A_t]^n \qquad (4.2)$$

$$\ln\left(-\frac{\partial A_t}{\partial t}\right) = n \ln A_t + \ln k_{app} \qquad (4.3)$$

Therefore, the slope of the linear fit of the plot between $\ln\left(-\frac{\partial A}{\partial t}\right)$ versus ln (A) gave the order of degradation kinetics for PNP and MO. The value of the slope of the plot between $\ln\left(-\frac{\partial A}{\partial t}\right)$ versus ln (A)is zero for PNP and MO degradation. Thus, the photo-Fenton degradation of PNP and MO on CF follows a pseudo-zero order rate kinetics. Figure 4.9b and Figure 4.10b shows $\left(\frac{A_t}{A_o}\right)$ against t plots for photo Fenton degradation of PNP and MO in the presence of SMNPS and CF catalyst. Here A_o and A_t are the initial and final concentrations of PNP and MO at time t = 0 and t respectively. Nearly perfect linear fits were obtained. The slope of the linear fits of the respective plot gives the pseudo-zero-order rate constant (k_{app}).

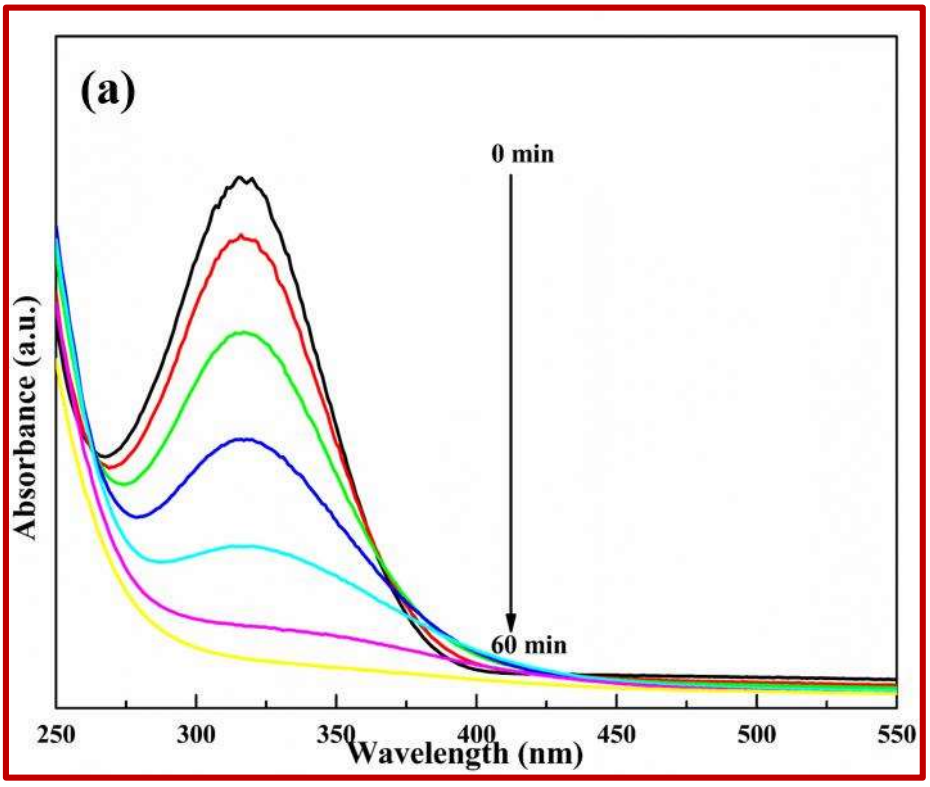

Figure 4.9 (a) UV-visible plots after regular intervals of the reaction time of photo Fenton degradation of PNP catalyzed by the CF nanocomposite.

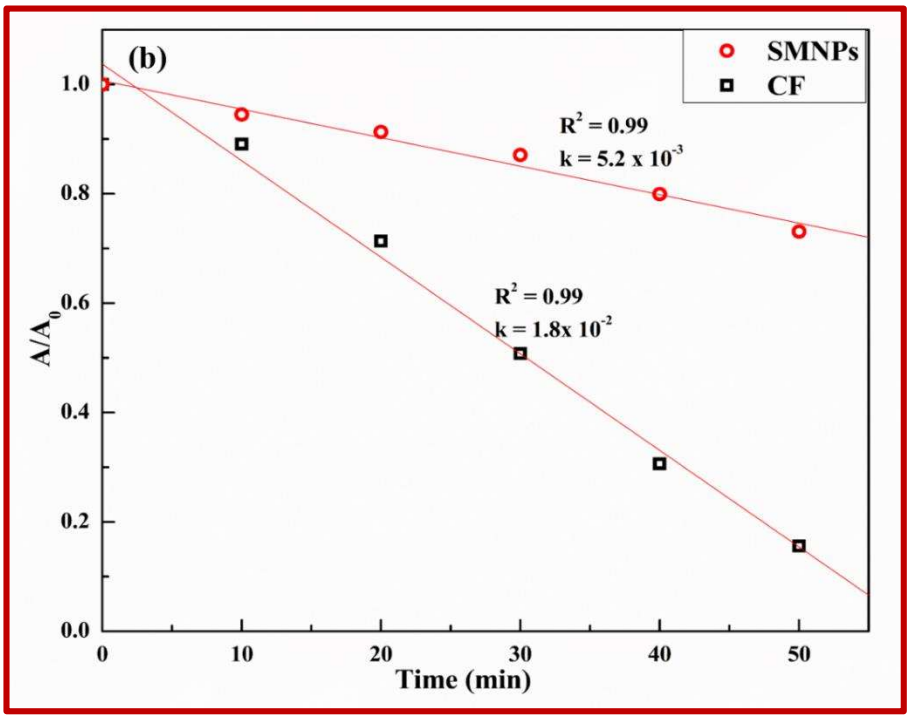

Figure 4.9 (b) The plots of (A/A_0) [absorbance (A) measured at λ_{max} 317 nm] versus time for PNP degradation reactions catalyzed by SMNPs and CF.

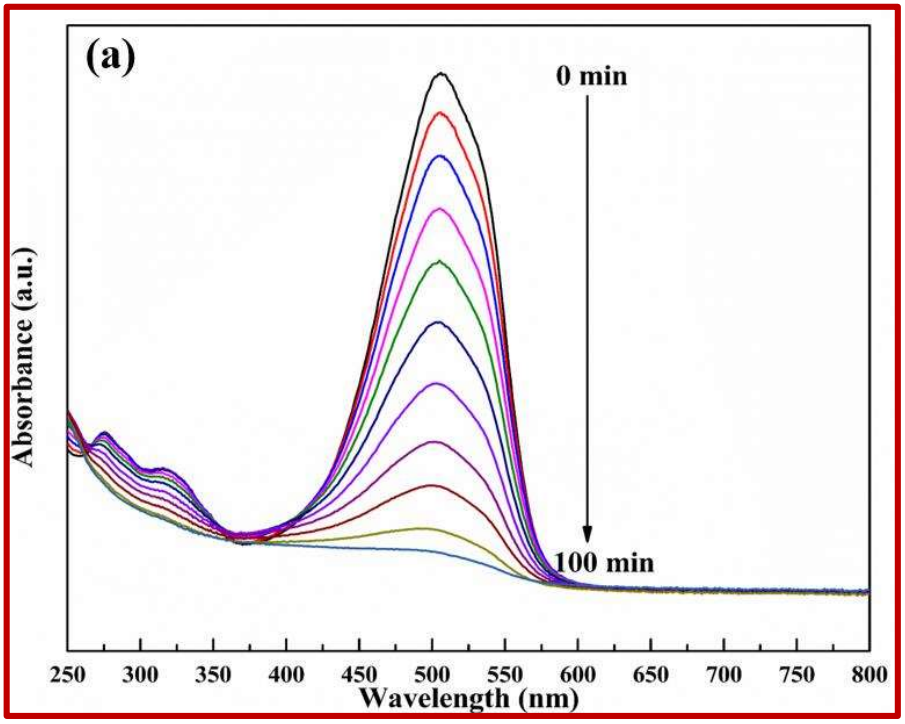

Figure 4.10 (a) UV-visible plots of photo Fenton degradation of MO at regular intervals of reaction time (under visible light conditions) catalyzed by CF.

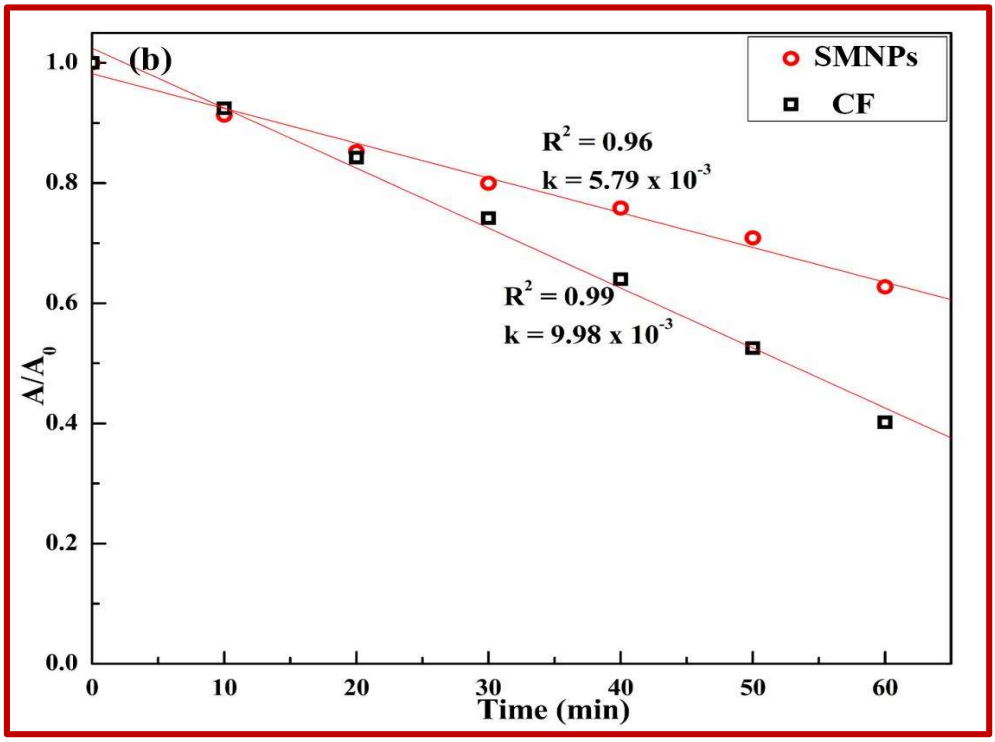

Figure 4.10 (b) The plots of (A/A_0) [absorbance (A) measured at λ_{max} 505 nm] versus time for (MO degradation) reactions catalyzed by SMNPs and CF.

The order of the reaction may be different when catalyzed by various catalysts. Quite clearly, the activities of diverse catalysts cannot be compared using the rate constant. Also, the rate constant does not consider the amount of the catalyst used in the reaction. Hence, the catalysts' activities were compared using turn over frequency (TOF) calculated by the following equation.

$$\text{TOF} = \frac{\text{Number of moles of reactant consumed} \times \text{yield}}{\text{Number of grams of catalyst} \times \text{time (minute)}} \qquad (4.4)$$

Table 4.1 compares the TOF value for photo-Fenton degradation of PNP in the presence of CF with other photocatalysts reported in the literature. Please note TOF values are rarely reported in the literature for photocatalysts, and consequently, the TOF values mentioned for references from the literature were calculated from the data provided in those research articles [Guo *et al.* (2013), Zhao *et al.* (2010), Ayodele *et al.* (2013), Hou *et al.* (2016), Qin *et al.* (2017)]. The comparison is restricted to photocatalysts that include

an iron oxide phase or Cu_2O as a component. Furthermore, the table consists of only those papers that provide enough data to calculate the respective TOF values. CF's TOF value is much higher than those exhibited by other catalysts except the Fe-TiO_2 photocatalyst [Zhao *et al.* (2010)]. But the Fe-TiO_2 photocatalyst is not a visible light catalyst, and it works only under UV light irradiation.

Table 4.1 Comparison of TOF values for Photo-Fenton degradation of PNP over different photocatalysts studied earlier in literature with the one investigated in this work.

Catalyst	**Light Source**	**TOF (moles gram^{-1} min^{-1}**	**Reference**
CF	Cool white LED (0.1470 W/cm^2, visible range light source)	1.17 x 10^{-5}	This work
$SiO_2/Fe_3O_4/C@TiO_2$	UV light from a Xenon lamp (CHFXQ 500 W)	5.65 x 10^{-6}	Hou *et al.* (2016)
$Fe_3O_4@SiO_2@ZnO$	300 W high-pressure Hg lamp	2.09 x 10^{-6}	Qin *et al.* (2017)
GO-Fe_2O_3	300W Dy Lamp (420nm visible light source)	2.5 x 10^{-6}	Guo *et al.* (2013)
Fe-TiO_2	UV lamp	1.23 x 10^{-5}	Zhao *et al.* (2010)
kaolinite supported ferric oxalate	UV lamp	4.6 x 10^{-9}	Ayodele *et al.* (2013)

**The TOF values from publications by authors other than ours are calculated from the data given in literature using Eq. 4.*

Table 4.2 compares the TOF value for photo-Fenton degradation of MO on CF with other photocatalysts reported in the literature [Xiao *et al.* (2019), Nayak *et al.* (2019), Omri *et al.* (2020)]. The TOF values mentioned for literature references were also

calculated from the data provided in those research articles. The MO degradation TOF value found over CF was found to be among the best reported to date in the literature.

Table 4.2. A comparison of the TOF values of various photocatalysts for photo-Fenton degradation of MO over CF nanoparticles.

Catalyst	**Light Source**	**TOF (moles gram^{-1} min^{-1})**	**References**
CF	Cool white LED (0.1470 W/cm^2, visible range light source)	2.66 x 10^{-5}	This work
Fe_2O_3/Au/SiO_2	300-W xenon lamp with a filter (λ>420 nm)	1.52 × 10^{-6}	Xiao *et al.* (2019)
ZnO/CuO nanocomposite	Cool white LED (0.980 W/cm^2, visible range light source)	1.44 x 10^{-6}	Nayak *et al.* (2019)
Fe- sand	UV light	1.47 x 10^{-5}	Omri *et al.* (2020)

**The TOF values from publications by authors other than ours are calculated from the data given in literature using Eq. 4.*

4.3.4 Recyclability test

The recyclability test of the CF photocatalyst was performed to check its stability. Figure 4.11 shows the recyclability experiment results of PNP degradation over CF nanoparticles. The CF photocatalyst shows good activity even after the fifth run.

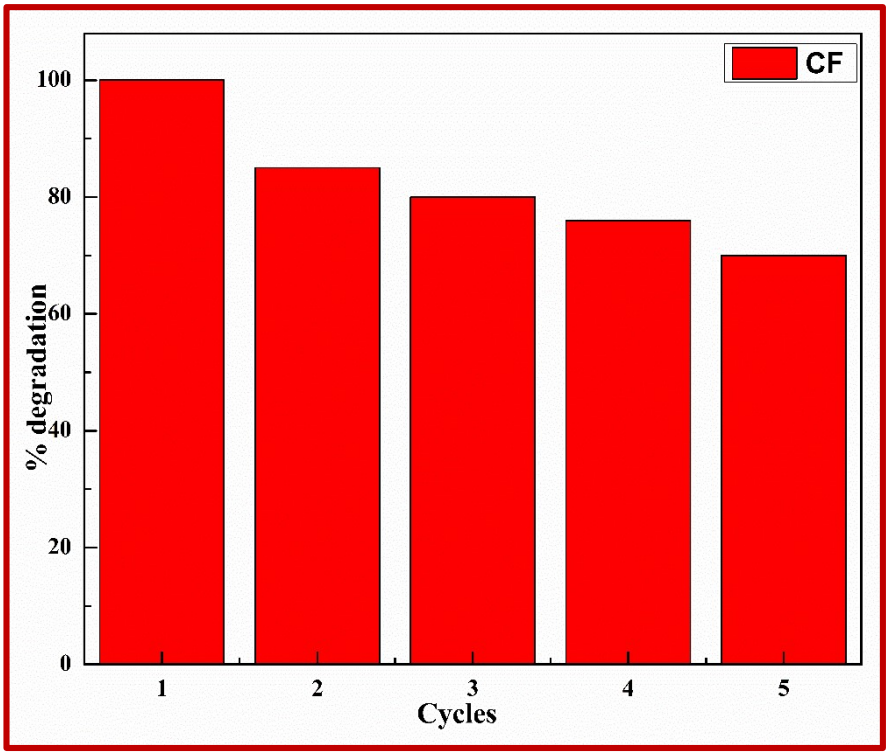

Figure 4.11 Five cycles of CF reusability results in histogram format for PNP degradation for 1 hour.

4.3.5 Proposed photocatalytic mechanism

In the prepared CF nanocomposite, the Cu_2O part is p-type, and the SM component an n-type semiconductor. Both components have bandgaps in the visible range and form a p-n heterojunction photocatalyst. On irradiation by visible light of suitable energy, both parts got photo-excited. The electrons excited to the CB of Cu_2O migrated to the CB of SM. Simultaneously, the holes in the VB of SM moved to the VB of the Cu_2O part. Thus, electrons concentrated on the CB of SM, and the holes were mainly on the VB of the Cu_2O component. The electrons on the CB of SM reduced H_2O_2 molecules to $OH\cdot$ and OH^- reactive species. The latter (OH^-) species got oxidized to $OH\cdot$ at the VB of the Cu_2O part of the p-n heterojunction. In subsequent steps, the generated $OH\cdot$ radicals degraded the organic pollutant molecules.

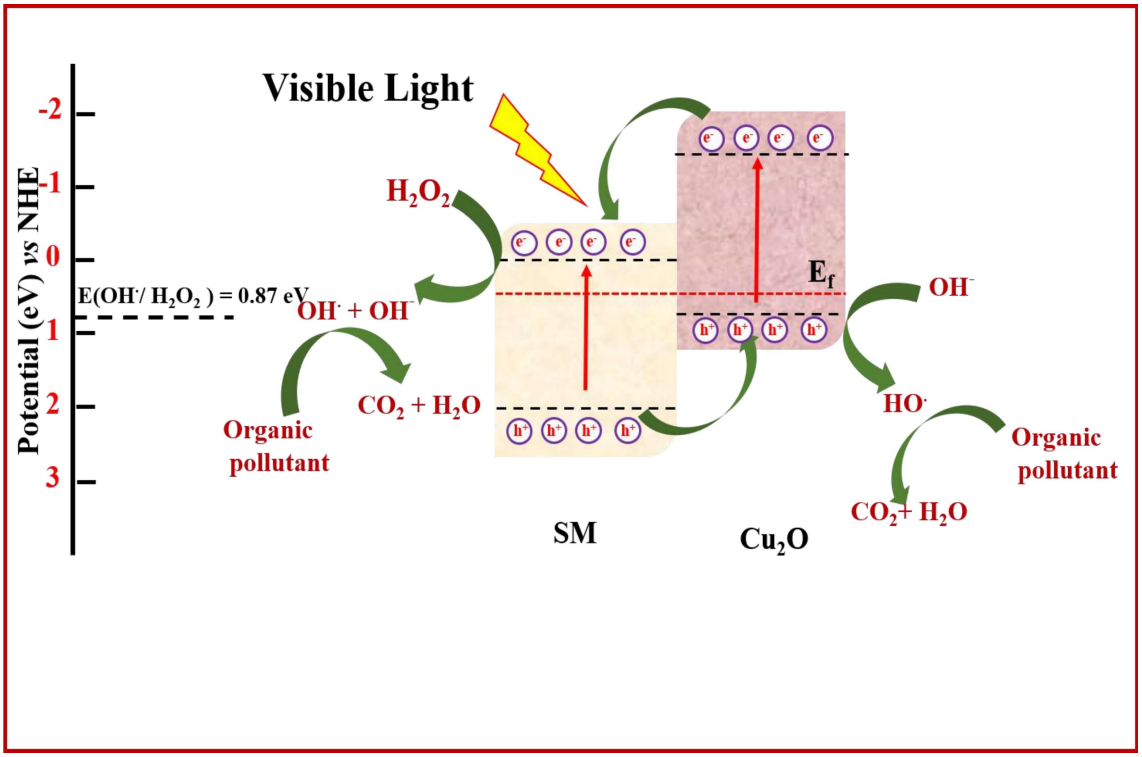

Figure 4. 12 Schematic representation of the proposed mechanism.

4.4 Conclusions

Discrete nanostructures of Cu_2O were precipitated over SM nanoparticles by a stage-wise preparation protocol. UV-visible diffuse reflectance spectrums established that both components of the nanocomposite have visible range band gaps. The nanocomposite exhibits efficient photo-Fenton activity for the degradation of PNP and MO. The prepared photocatalyst also demonstrated effective magnetic recyclability. Furthermore, Mott-Schottky measurements showed that the two parts form a p-n heterojunction. Nyquist plots (from electrochemical impedance spectroscopy) established proficient charge transfer and separation between the nanocomposite parts. Photo-excited electrons migrated to the CB of the SM part, while the holes got transferred to the Cu_2O portion. The generated hydroxyl radicals caused the degradation of PNP and MO.